Terahertz EPR spectroscopy using a 36-tesla high-homogeneity series-connected hybrid magnet

Thierry Dubroca[1,*], Xiaoling Wang[1,2,†], Frédéric Mentink-Vigier[1], Bianca Trociewitz[1], Matthieu Starck[3], David Parker[3], Mark S. Sherwin[4], Stephen Hill[1,2,5], J. Krzystek[1,*]

1. National High Magnetic Field Laboratory, Florida State University, Tallahassee, FL 32310, USA
2. Center for Molecular Magnetic Quantum Materials, University of Florida, Gainesville, FL 32611, USA
3. Department of Chemistry, University of Durham, Durham DH13LE, UK
4. Department of Physics, University of California Santa Barbara, CA 93106, USA
5. Department of Physics, Florida State University, Tallahassee FL 32306, USA

*To whom correspondence should be addressed: dubroca@magnet.fsu.edu; krzystek@magnet.fsu.edu

[†]Present address: Department of Chemistry and Biochemistry, California State University East Bay, Hayward, CA 94542

Abstract

Electron Paramagnetic Resonance (EPR) is a powerful technique to study materials and biological samples on an atomic scale. High-field EPR in particular enables extracting very small *g*-anisotropies in organic radicals and half-filled 3d and 4f metal ions such as Mn^{II} ($3d^5$) or Gd^{III} ($4f^7$), and resolving EPR signals from unpaired spins with very close *g*-values, both of which provide high-resolution details of the local atomic. Before the recent commissioning of the high-homogeneity Series Connected Hybrid magnet (SCH, superconducting + resistive) at the National High Magnetic Field Laboratory (NHMFL), the highest-field, high-resolution EPR available was limited to 25 T using a purely resistive "Keck" magnet at the NHMFL. Herein, we report the first EPR experiments performed using the SCH magnet capable of reaching the field of 36 T, corresponding to an EPR frequency of 1 THz for g = 2. The magnet's intrinsic homogeneity (25 ppm, that is 0.9 mT over 1 cm diameter, 1 cm length cylinder) was previously established by NMR. We characterized the magnet's temporal stability (5 ppm, which is 0.2 mT over one-minute, which is the typical acquisition time) using 2,2-diphenyl-1-picrylhydrazyl (DPPH). This high resolution enables resolving the weak *g*-anisotropy of 1,3-bis(diphenylene)-2-phenylallyl (BDPA), $\Delta g = 2.5 \times 10^{-4}$ obtained from measurements at 932 GHz and 33 T. Subsequently, we recorded EPR spectra at multiple frequencies for two Gd^{III} complexes with potential applications as spin labels. We demonstrated a significant reduction in line broadening in Gd[DTPA] attributed to second order zero field splitting by analogy to similar systems, and a resolution enhancement of *g*-tensor anisotropy for Gd[sTPATCN]-SL.

Keywords: Electron Paramagnetic Resonance, EPR, high-field EPR, terahertz EPR, organic radical, BDPA, g-tensor, gadolinium spin labels

1. Introduction

One of the most important advantages of high-field electron paramagnetic resonance (HFEPR) is an increased resolution[1] of spectral features occurring due to g-factor anisotropy compared to commercially available (X, Q, W or G-band) EPR spectrometers. In this respect, EPR is analogous to NMR which benefits from increased resolution at high fields which helps resolve the chemical shift anisotropy in NMR. Resolving the anisotropy of the *g*-tensor is of great importance in many naturally-occurring organic radicals. Indeed, such chemical species typically contain only light atoms (C, H, N, O), where the spin-orbit interaction, which is responsible for the phenomenon of *g*-anisotropy, is weak, and that anisotropy remains unresolved at conventional (i.e., low) microwave frequencies and magnetic fields. The determination of the g-anisotropy provides unique insights of the orbital composition and thus the nature and geometry of paramagnetic centers.

Other compounds that benefit from high fields are spin systems with total spin numbers $S > ½$. The spin Hamiltonian for such paramagnetic species includes a zero-field splitting (ZFS) interaction, in addition to the electronic Zeeman term, which is equivalent to quadrupolar interactions in Nuclear Magnetic Resonance (NMR). This interaction is often present in metal ions such as Mn^{II} and Gd^{III}, both of which have half-filled shells ($3d^5$ and $4f^7$, respectively) and the advantage offered by high fields is different from the case of organic radicals described above. In the presence of ZFS, the degeneracy of the spin projection states is lifted even in the absence of external magnetic field, B_0. The central single-quantum transition of species with half-integer spin states ($m_S = –½ \rightarrow m_S = +½$) is broadened by ZFS at the second-order in the perturbation theory, as opposed to the side transitions between states of higher $|m_S|$, which are broadened at the first order. The spectral broadening of the central transition scales inversely with B_0, in contrast to the side transitions that experience a field-independent broadening. The resolution improves with increasing field and the ZFS can be used to obtain intricate structural sensitivity to the surrounding ligand environment. Complexes of Gd^{III}, that possess seven unpaired electrons in the ground state ($S = 7/2$), have found applications in two main areas: as contrast agents for Magnetic Resonance Imaging[2] and as spin labels for the study of protein conformations.[3] The narrowing of their central transitions with increasing magnetic field can be dramatic, as previously reported on several different Gd^{III} spin labels from Q-band EPR (34 GHz, ~1 T) to G-band (240 GHz, ~8 T).[4] The width of the central line in the EPR spectrum carries special importance in the use of Gd^{III} as a spin label. Critical parameters in Double Electron-Electron Resonance (DEER) or Pulsed Electron Double Resonance (PELDOR) experiments such as sensitivity and modulation depth depend on it.[5] Furthermore, the Gd^{III} linewidth itself can be used as a sensitive probe of dipolar interactions with nearby spins,[6,7] which has been exploited in the recent demonstration of Time-resolved Gd-Gd Electron paramagnetic Resonance (TiGGER) to measure triggered conformational dynamics of an optogenetic protein upon light activation.[8]

In this work, we present a new electron magnetic resonance spectrometer based on the 36 T high homogeneity series connected hybrid (SCH) magnet commissioned at the National High Magnetic Field Laboratory, in Tallahassee, Florida, USA.[9] In the first section we characterize the instrument's temporal field stability. Following that, we present EPR spectra of both low-spin radicals (as solids) and high-spin Gd^{III} complexes (as frozen solutions) at frequencies just below 1 THz, demonstrating the ability to resolve very small *g*-anisotropy and record very narrow linewidths of the central line in Gd^{III} spectra, thus demonstrating the resolving power of the instrument. Finally, the current limits and future improvements of the instrument are discussed.

2. Experimental

2.1. Spectrometer design

The layout and schematics of the HFEPR spectrometer based on the recently commissioned 36 T SCH magnet[9] are shown in Figure 1. This magnet is composed of a superconducting outsert coil and normal metallic conductor insert coils connected in series. The series design was chosen to decrease ripples of the power supply thanks to the large inductance of the superconducting coil, thus providing high temporal stability. Additionally, the coils were designed and assembled in a way to create a high-homogeneity field at their center: 25 ppm in the volume limited to 1 cm diameter, 1 cm height, with a magnet bore diameter of 40 mm to accommodate cryostats, shims, and probes. Finally, the magnet is capable of fast ramp rates, up to 1 T/min from 0 to 36 T. The other components of the EPR spectrometer are a solid-state THz source (Virginia Diodes Inc., USA), an indium antimonide bolometer (Thomas Keating Ltd., England), an in-house built transmission probe, waveguides connecting the probe to the source, and a cryostat (Janis, USA) to lower the temperature. The outer, superconducting, coil of the SCH magnet has a large bore which generates a significant stray field, requiring long waveguides to allow the source and detector to be placed in reasonably low stray fields to operate without disruption. Two separate microwave multiplication chains are available for this instrument. One source's output is 40 mW in the 305-325 GHz range, which can be extended with the use of a passive tripler to produce 910-960 GHz microwaves with 1 mW output power. The second source provides about 0.5 mW output power in the 610-640 GHz band. To transmit the THz signal from the source to the sample and finally to the detector, a smooth wall horn in combination with a series of waveguides and mirrors is employed. Depending on the source frequency a rectangular transition is used to convert to a WR10 rectangular guide, which is connected to a WR10 to circular horn (10 mm ID). The THz signal is then transmitted via smooth wall waveguides (10 mm ID) in straight sections. At each bend, a mirror is used to re-direct the THz beam. Inside the probe, the beam travels down via a vertical waveguide to the sample before being re-directed upwards via a second waveguide using a combination of off-axis parabolic mirrors. At the top of the probe two flat mirrors are used, one for the input from the

source and one for the output towards the bolometer. A classic phase-sensitive detection scheme using a lock-in amplifier is employed in order to demodulate the EPR signal generated via a modulation coil located around the sample. Finally, a temperature control system consists of a bucket-type cryostat which can be either filled with liquid nitrogen or liquid helium and a strip heater located around the probe head allows temperature to be controlled between ~1.5 and 170 K. The probe is placed in a sleeve, immersed in the liquid cryogen, that is filled with helium gas at low pressure, serving as a heat exchange.

At the highest frequencies, the sample's dielectric absorption has a strong influence on the signal-to-noise-ratio. The THz wave transmission through the sample follows an exponential decay while, in the absence of absorption, the signal strength scales linearly with the number of spins (or sample volume). Thus, the preferred sample geometry is a large-diameter cylinder (8.4 mm ID Teflon cup, Figure 1) with a small thickness to minimize the absorption while keeping the volume relatively large. We found that, for frozen aqueous solutions, the optimal thickness was about 1 mm, which meant that the sample volume was about 50 μL. In the case of loose powder, a Teflon cap (not shown) is used.

The NHMFL allocates magnet time on the SCH one week (4 and a half working days) at a time, for a total of about 40 hours. Therefore, due to the limited time available on this shared magnet and the significant operating costs, samples are selected and optimized at lower fields (5 – 15 T) in traditional superconducting magnets. During the SCH magnet operation, for safety reasons, no one is allowed on the magnet platform at fields above 18 T (see Figure 1). We therefore typically perform preliminary experiments at an intermediate field (11 T, or 310 GHz for g = 2) to optimize the probe, mirrors and waveguide positions relative to the source.

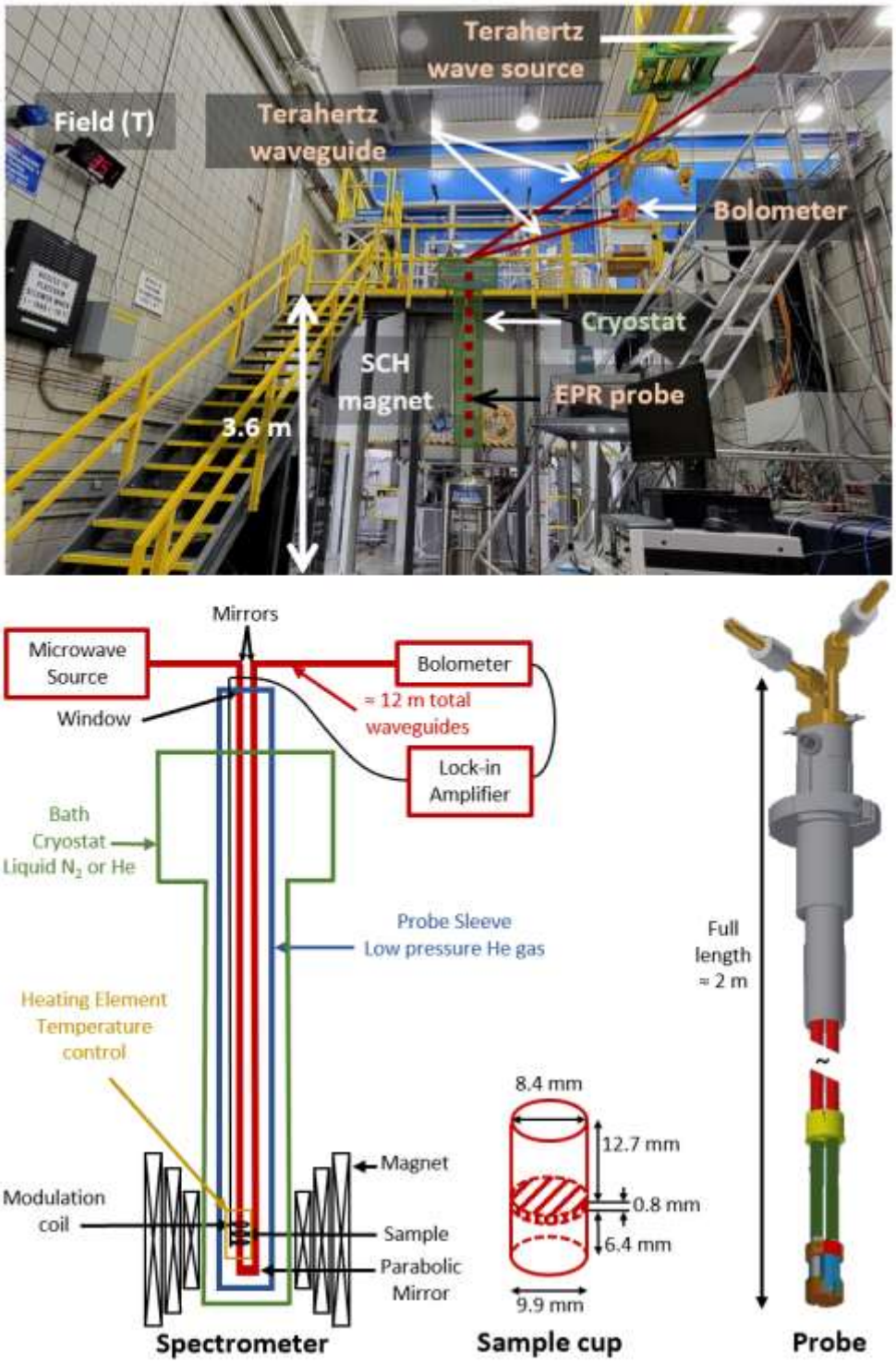

Figure 1. (Top) Photograph of the EPR spectrometer based on the SCH magnet. The main components of the spectrometer are labeled. (Bottom) schematic of the spectrometer, sample cup geometry and 3D rendering of the home-built probe. Spectrometer specifications: field up to 36 T with a sweep rate up to 1 T/min; field homogeneity of 25 ppm (1 cm diameter, 1 cm tall volume); temporal stability of 5 ppm (1 min time scale); available frequencies of 305 – 325, 610 – 640, and 910 – 960 GHz; temperature 1.5 – 300 K; typical sample volume of 10 to 200 μL; and a total waveguide length of ≈ 10 m. At the time of the photograph the field was at 35.1 T.

2.2. Sample preparation

Several samples were employed in this work, each one prepared to meet a specific goal. First, about 1 mg of pure DPPH (2,2-diphenyl-1-picrylhydrazyl) solid (powder) was spread on the bottom of a 6 mm Teflon cup. This sample was meant to produce a very strong signal so that it could be used to characterize the temporal stability of the spectrometer. The second sample was BPDA encapsulated in polystyrene at a relatively low concentration (1.7 mM) to avoid electron spin-spin interactions. Polystyrene pieces were cut and fitted into a Teflon cup (6 mm diameter and 5 mm tall) occupying a volume of 130 µL. Finally, gadolinium complexes were prepared in fully deuterated 1:1 (v/v) water-glycerol solutions. Deuteration was employed to minimize electron-nuclear spin relaxation due to ^{1}H hyperfine coupling, while a low concentration was again chosen (500 µM) to minimize electron spin-spin dipolar coupling. The solutions were poured into Teflon cups with 8 mm inner diameter and filled to 1 mm height, occupying a volume of 50 µL. Separate samples were prepared of the Gd[sTPATCN]-SL[5] and Gd[DTPA] complexes[5,10] shown in Scheme 1. Gd[DTPA] was purchased from Millipore Sigma. Gd[sTPATCN]-SL was synthesized by Matthieu Starck and David Parker and is from the same batch used in Ref.[8]

Scheme 1. Structures of the Gd complexes used in this study.

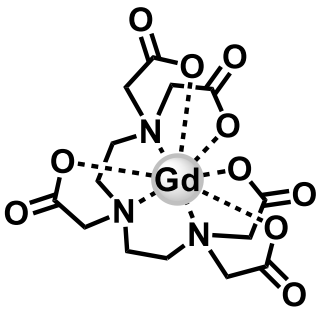

Gd[DTPA]
Gadolinium diethylenetriamine-pentaacetate

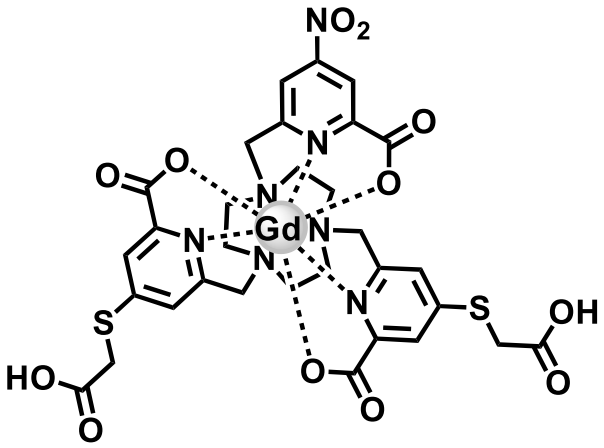

Gd[sTPATCN]-SL
Gadolinium 6,6'-((7-((6-carboxylato-4-nitropyridin-2-yl)methyl)-1,4,7-triazacyclonane-1,4-diyl)bis(methylene))bis(4-((carboxylatomethyl)thio)picolinate

3. Results and Discussion

3.1. Spectrometer characterization

In order to characterize the spectrometer from the point of view of suitability for high-resolution EPR, we first measured a spectrum of DPPH at 936.00 GHz and 79 K, Figure 2a. As previously described by Krzystek et al.,[11] DPPH reveals an underlying structure at high fields due to both intrinsic *g*-anisotropy and a complex sample composition involving the crystallization solvent; we did not pursue this subject in the current study. In order to evaluate the temporal stability of the magnet, we recorded the EPR amplitude of the resonance at the steepest slope (Figure 2a) of its derivative-shaped spectrum as a function of time. Figure 2b displays both the field and EPR signal strength temporal variations. It should be noted that the magnetic field is calculated from measuring the current generated by the power supply using a calibration curve obtained previously from NMR. We found the accuracy of this value to be ca. ±100 mT (± 3000 ppm) at 33 T. In Figure 2b both data sets are strongly correlated, demonstrating that the EPR signal stability is correlated with the temporal stability of the power supply. The temporal stability is about 5 ppm (or 0.2 mT at 33 T) over the typical spectrum acquisition time scale (1 min). Note that for longer acquisition times (10 mins) the temporal stability is about 10 ppm. The temporal field variation is attributed to the magnet power supply and water-cooling regulation. Another important parameter to consider with this spectrometer is the field homogeneity, which had been previously measured to be 25 ppm (or ~1 mT at 33 T) for a 1 cm diameter × 1 cm height volume.[9] The SCH is most inhomogeneous in the XY plane (perpendicular to the direction of THz beam propagation and the applied field). The field inhomogeneity for the disk-shaped sample (8.4 mm diameter) is just under 25 ppm from the field map[9].

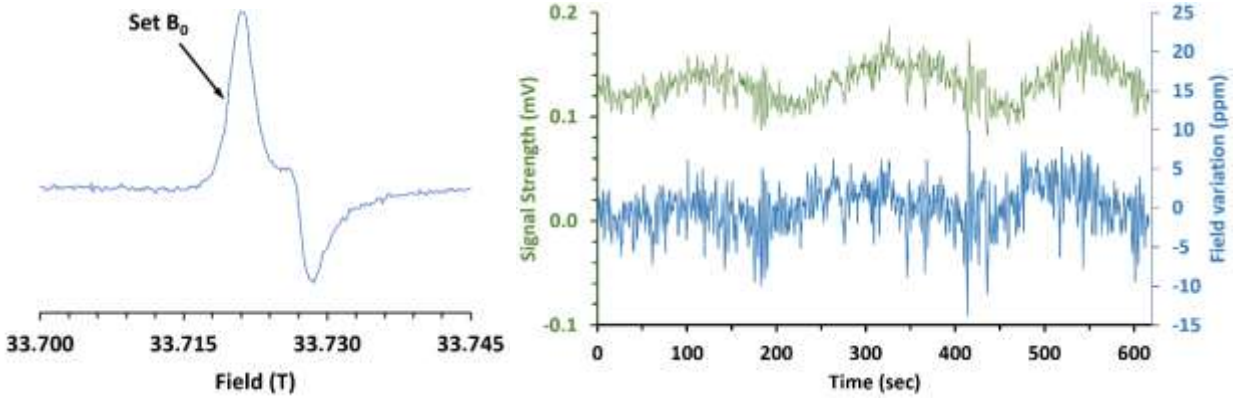

Figure 2. (a) EPR spectrum of DPPH recorded at 936.00 GHz and 79 K. (b) EPR signal amplitude at the maximum slope of the EPR spectrum (green trace) and magnetic field variation calculated from the current supplied by the magnet power supply (blue trace) as a function of time. Note: the field value (B_0) set at the maximum slope of the EPR spectrum is marked by an arrow on (a). The acquisition time was set to 0.5 sec per point.

3.2. THz EPR of a low-spin (S = 1/2) system

Natural organic radicals are commonly found in coal,[12] carbonaceous matter[13–15] and in biological matter. In the latter, they have been associated with specific diseases.[16] Synthetic radicals are used in many applications, most recently as polarizing agents in Dynamic Nuclear Polarization (DNP).[17–24] A typical organic radical producing a narrow EPR resonance is BDPA (1,3-bis(diphenylene)-2-phenylallyl). This radical contains only carbons and hydrogen atoms which results in very weak spin-orbit coupling. As a consequence, its *g*-anisotropy is very weak, with *g*-tensor components close to the free electron value (~2.0023). Nonetheless, a *g*-anisotropy was estimated at 140 GHz (5 T) in earlier work,[25] where the following principal values were reported: g_x = 2.00263, g_y = 2.00260, and g_z = 2.00257, for BDPA in polystyrene (1% weight concentration) at room temperature. Thus, the *g*-anisotropy reported was $\Delta g = g_x - g_z = 6 \times 10^{-5}$.

We carried out EPR measurements on a similar sample (1.7 mM BDPA in polystyrene) to demonstrate the resolution capabilities of the newly built spectrometer. The spectrum and its fit, using EasySpin[26] (v5.2.35, function "pepper", isotropic g-strain of 0.8×10^{-4}, Gaussian and Lorentzian linewidth of 0.2 mT) are shown in Figure 3 for a frequency of 936.00 GHz, indicating a sizeable axial anisotropy that is undetectable at lower frequencies. The *g*-values obtained through the fits are: g_x = 2.00265, g_y = 2.00263 and g_z = 2.00240, with an uncertainty of ±0.00001 in each component. While neither the absolute values nor that of the average, $g_{iso} = 1/3\ (g_x + g_y + g_z)$, can be precisely determined due to the inaccuracy in reading the magnetic field, the differences in the *g*-values are precise. In particular, the *g*-anisotropy Δg amounts to ca. 2.5×10^{-4}, i.e., it is about five times larger than the one previously reported.[27] That work, however, was performed at much lower field (5 T) with the anisotropy barely visible in the spectrum. The newly determined *g*-tensor values was compared to Density Function Theory (DFT) predictions carried out using Orca 5.0.1[28] after optimizing the BDPA structure with the PBEh-3c approach.[29] The DFT calculations were performed using the functional PBE0[30] and def2-TZVP[31] as basis. The predictions, g_x = 2.00269, g_y = 2.00263, and g_z = 2.00239 ($\Delta g = 3 \times 10^{-4}$), are very close to the experimentally fitted values presented above, thereby highlighting the resolving power of the spectrometer.

BDPA is a relatively stiff molecule thanks to its conjugated bond network. In the measured polystyrene matrix, it is believed that the molecular geometry is likely unaffected by the soft polymer. Therefore, the *g*-anisotropy is likely the same for BDPA molecules in solution. Its *g*-anisotropy is not only of academic interest, it also plays an important role in the longitudinal (T_1) relaxation of the electron spin.[32] Therefore, these measurements should enable prediction of the relaxation rates of BDPA radicals in a variety of solvents at high fields, information that could be on interest for a range of applications, from spin labeling to quantum information sciences.

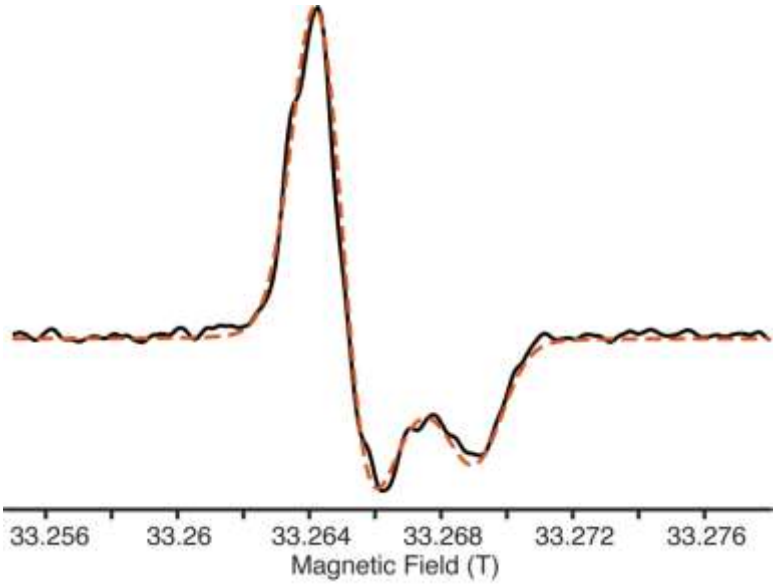

Figure 3. EPR spectrum of BDPA in polystyrene measured at 936.00 GHz and 82 K [solid back line: 9-point average smoothing (~ 0.8 mT) filter was applied to the collected data]. The red dashed line is the simulated spectrum using the following *g*-tensor principal values [g_x, g_y, g_z] = [2.00265, 2.00263, 2.00240] with an uncertainty of ±0.00001 for each value. Note: magnetic field values were shifted arbitrarily by –0.1955 T from the current-calibrated values to yield an average value consistent with previous publications and DFT predictions. The simulations were carried out with EasySpin v5.2.35 and the function "pepper". An isotropic g-strain of 0.8×10^{-4} was used to reproduce the lineshape as well as a mixture of Gaussian and Lorentzian linewidth of 0.2 mT respectively.

3.3. THz EPR of high spin (S = 7/2) systems

To study high-spin (S > ½) systems, we chose two coordination complexes of gadolinium, abbreviated as Gd[DTPA] and Gd[sTPATCN]-SL (Scheme 1). In the following, we concentrate on measuring the width of the central transition in each of these complexes, evaluating both the concentration limit in a frozen aqueous solution, and the resolution limit of the spectrometer and the SCH magnet.

Gd[DTPA] in frozen solution produces a single approximately isotropic resonance at any frequency, corresponding to the central (m_S = –½ → m_S = +½) transition of the S = 7/2 multiplet (Figure 4). The Full Width at Half Maximum (FWHM) linewidth of that transition follows the trend observed previously at lower frequencies (36 – 240 GHz),[4,33] becoming narrower with increasing frequency (field), demonstrating the effect of the decreasing second-order ZFS interaction (Figure 5 and Table 1). The linewidths (FWHM) were extracted using single line fits with either a Gaussian or Lorentzian distribution and taking into account the dispersion. The FWHM linewidth of Gd[DTPA] at operating frequencies and temperatures of 310.80 GHz (35 K), 614.88 GHz (60 K), and 932.40 GHz (80 K) is 3.82, 2.67, and 1.52 mT, respectively. (In order to optimize the signal intensity, temperature was chosen for each complex and each frequency such that the m_S = ±½ levels were at their maximum population. Fitting this resonance with a single set of spin Hamiltonian parameters (g-values and ZFS parameters) was unsuccessful, most likely

due to a presence of two different spin species, whose nature is not clear. The second species might be responsible for the low-field shoulder observed at 932.40 GHz (Figure 4).

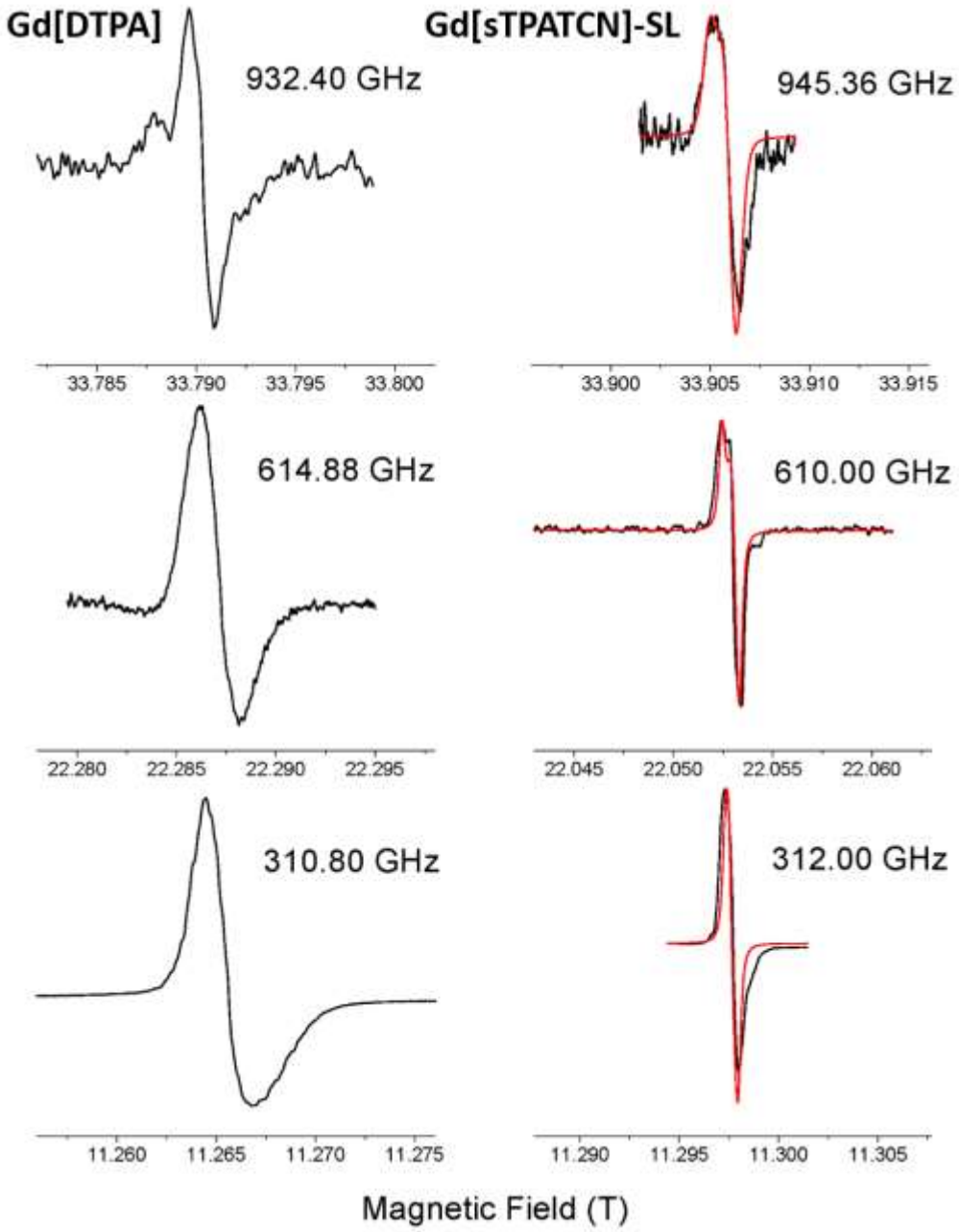

Figure 4. EPR spectra of Gd[DTPA] (left column, at 80, 60 and 35 K, from top to bottom, respectively) and Gd[sTPATCN]-SL (right column at 79 K throughout, black traces) and simulated spectra (red traces for Gd[sTPATCN]-SL only). Gd[sTPATCN]-SL spectra were simulated with the same set of parameters: $\boldsymbol{g}$ = [1.9920, 1.9920, 1.9921] and D = 0.016 cm^{-1}. An angle of 56 degrees between the $\boldsymbol{g}$ and ZFS tensors was assumed. Note (1): to ease comparisons, all spectra are plotted on the same (x-axis) scale. Note (2): at the highest fields, the spectra are averages of 20 and 36 single scans, for Gd[DTPA] and Gd[sTPATCN]-SL, respectively. The simulations were carried out with EasySpin v5.2.35 and the function "pepper". An isotropic g-strain of 0.2×10^{-4} as well as a mixture of Gaussian and Lorentzian linewidth of 0.15 mT respectively was used to reproduce the lineshape.

Gd[sTPATCN]-SL, measured also in a frozen solution, similarly produces a single isotropic resonance in the lower range of frequencies, showing the expected narrowing of the linewidth between 64.000 and 240.00 GHz (from 1.18 to 0.72 mT FWHM, Figure 4 and Table 1). However, this resonance broadens at 610.00 GHz (0.9 mT FWHM) and 945.36 GHz (1.45 mT FWHM) compared with lower frequencies. The EPR spectra of Gd[sTPATCN]-SL also shows a structure (Figure 4b), which we attribute to a partly resolved g-anisotropy based on simulations. We analyzed the spectra using the following spin Hamiltonian:

$$\widehat{H} = \beta \vec{S} \boldsymbol{g} \vec{H} + D\left(S_z{}^2 - \frac{1}{3}S(S+1)\right)$$

where *ß* is the Bohr magneton, g represents the $\boldsymbol{g}$-tensor, S is the spin number (7/2), S_z its z-component, and D is the axial zero-field splitting (ZFS) tensor parameter.

We were able to fit the EPR spectra of Gd[sTPATCN]-SL at 312.00, 610.00 and 945.36 GHz using the following set of parameters: $\boldsymbol{g}$ = [1.9920, 1.9920, 1.9921] and D = 0.016 cm^{-1}. The spectrum was fitted using EasySpin[26] v5.2.35 with the function "pepper" using an isotropic g-strain of 0.2×10^{-4} as well as gaussian and Lorentzian linewidths of 0.15 mT. An angle of 56 degrees between the $\boldsymbol{g}$ and ZFS tensors had to be assumed to reproduce the experimental spectrum. The agreement between the experiment and the simulation is reasonable but fitting to the data accurately is challenging. Compared to Gd[DTPA] with the D and E parameters of 0.048 and 0.0013 cm^{-1},[10] Gd[sTPATCN]-SL has smaller ZFS due to a higher symmetry of its coordination sphere.[5] We interpret the linewidth variation with the frequency in the case of Gd[sTPATCN]-SL as follows: the central transition narrows with field due to 2nd order ZFS up to about 400 GHz, then the overall width starts to increase linearly with field on account of g-anisotropy (or g-strain) which eventually dominates at the highest fields and frequencies. An alternative explanation is given in Figure 5: the narrow linewidth of the Gd[sTPATCN]-SL sample is approaching the spectrometer's resolution limit. We calculated this limit for the particular sample size and shape from NMR data[9] obtained on the SCH magnet homogeneity (0.25, 0.5 and 0.75 mT at 11, 22 and 33 T, respectively) and temporal variation (5 ppm) over the time scale of a field sweep (≈ 1 min). The resulting minimal resolution is 0.3, 0.6 and 0.9 mT for 11, 22 and 33 T. At the highest frequency (945.36 GHz) an additional broadening of the resonance line might have been caused by overmodulation, which was necessary because of the very low signal-to-noise ratio.

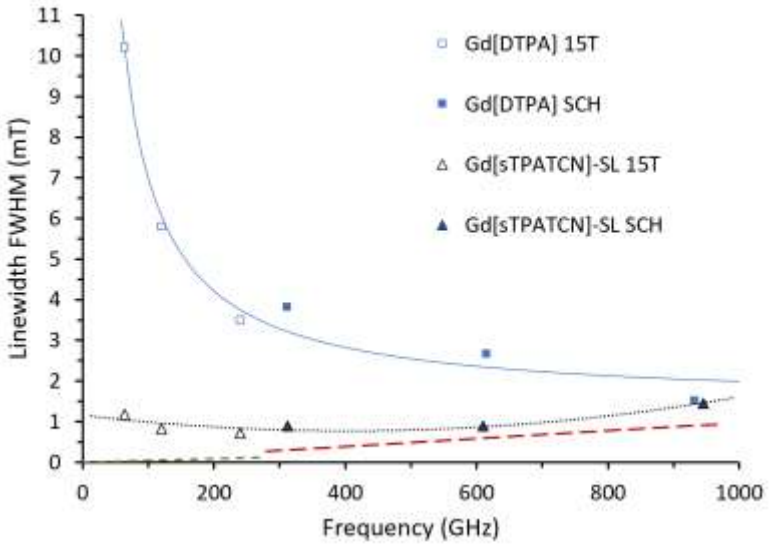

Figure 5. Frequency dependence of the width of the central line of Gd[DTPA] (squares) and Gd[sTPATCN]-SL (triangles) at cryogenic temperatures (up to 80 K) based on data collected with the SCH magnet (solid symbols), and a superconducting 15 T magnet (hollow symbols). The black dash line is a guide to the eye, while the solid blue line represents a one over frequency function. The red dashed line represents the limit of resolution of the SCH magnet, that is, the field homogeneity and stability limit as calculated from NMR mapping of the magnet and sample dimensions, while the green dash line represents the resolution of the superconducting 15 T magnet also estimated from the sample dimensions (smaller than in the SCH magnet case) and magnet field homogeneity (20 ppm).

Table 1. FWHM linewidth values in mT of Gd[DTPA] and Gd[sTPATCN]-SL in 500 µM deuterated water-glycerol solutions observed at various frequencies and cryogenic temperatures. The resolution limit of the spectrometer based on sample size, field homogeneity and field stability, in mT, is also added for comparison.

Frequency (GHz)	**64.000***	**120.00***	**240.00***	**310.80**	**614.88**	**932.40**
Gd[DTPA]	10.2	5.8	3.5	3.82	2.67	1.52
Frequency (GHz)	**64.000***	**120.00***	**240.00***	**312.00**	**610.00**	**945.36**
Gd[sTPATCN]-SL	1.18	0.83	0.72	0.89	0.90	1.45[#]
Resolution limit	0.03	0.06	0.12	0.3	0.6	0.9

* EPR spectra at 64, 120, and 240 GHz were obtained using a 15 T-based spectrometer under conditions comparable to those using the SCH-based instrument.

[#] The field modulation amplitude (0.5 mT) was set higher than optimal due to the very low signal-to-noise ratio.

4. Conclusions and future work

This work presents a high-resolution EPR spectrometer operating at frequencies up to 1 THz and field up to 36 T with a resolution of about 30 ppm. This ultra-high resolution has allowed us to precisely determine the g-anisotropy of the BDPA radical in polystyrene as well as the g- and *D*-values of the gadolinium complex Gd[sTPATCN]-SL. The multi-frequency capability of the instrument also allowed us to follow the frequency dependence of the width of the central transition of the two Gd^{III} compounds, Gd[DTPA] and Gd[sTPATCN]-SL. While for Gd[DTPA] the linewidth decreases with increasing frequency, as it does in previously studied Gd^{III} compounds, the trend in Gd[sTPATCN]-SL is reversed

above about 400 GHz, with the linewidth increasing with increasing frequency. This can be attributed to the *g*-anisotropy influencing the linewidth for systems with intrinsically narrow linewidths, although with a caveat that we approach the spectrometer's resolution limit for such narrow lines. The result that the linewidth of Gd[sTPATCN]-SL does not seem to follow the 1/B scaling above about 200 GHz, and the hint of a *g* anisotropy, will be important for developing quantitative biological distance measurements based on very high field EPR spectroscopy of proteins tagged with Gd^{III} spin labels, like time-resolved Gd-Gd electron paramagnetic resonance (TiGGER).[8]

Although this new instrument provides exceptional resolution, its sensitivity at near-terahertz frequencies is not entirely satisfactory, mainly because of the immense length of cylindrical light-pipes that is necessitated by the strong fringe field produced by the magnet. Therefore, future developments will focus on slower sweep rates to allow longer averaging times, an increase in B_1 field through use of a focusing horn, which will also allow us to work with smaller samples and enable a higher field homogeneity across the sample which will, in turn, improve the resolution. Finally, passive ferroshims could be built, similar to the ones developed by the NMR users of the same magnet,[9] to improve the field homogeneity. In the long term, a quasi-optical THz beam propagation system will be employed instead of the current simple cylindrical tubes and mirrors. This should significantly increase the B_1 field at the sample, which would provide a higher sensitivity.

5. Request for information

The National High Magnetic Field Laboratory encourages interested parties to contact the authors to learn about the process to obtain access to this new instrument.

6. Data availability

The data presented here will be made available on the osf.io repository at the time of publication.

Declaration of competing interest

The authors declare that they no known competing financial interests or personal relationships that could have appeared to influence the work reported in this paper.

Acknowledgement

Dr. Mykhaylo Ozerov is acknowledged for sharing his technical know-how relative to instrumentation and low-loss transmission at terahertz frequencies. S.H. and T.D. acknowledge support from the National Science Foundation, award CHE-2203405. X.W. and S.H. acknowledge support from the Center for Molecular Magnetic Quantum Materials (M2QM), an Energy Frontier Research Center funded by the US

Department of Energy, Office of Science, Basic Energy Sciences under Award DE-SC0019330. This work was performed at the National High Magnetic Field Laboratory which is supported by the National Science Foundation (cooperative agreements DMR-1644779 and DMR-2128556) and the state of Florida. M. S. S. acknowledges support from NSF-MCB-2028560.

References

1. Stoll, S. *et al.* Hydrogen bonding of tryptophan radicals revealed by EPR at 700 GHz. *J. Am. Chem. Soc.* **133**, 18098–18101 (2011).
2. Kim, H.-K., Lee, G. H. & Chang, Y. Gadolinium as an MRI contrast agent. *Future Med. Chem.* **10**, 639–661 (2018).
3. Giannoulis, A., Ben-Ishay, Y. & Goldfarb, D. Characteristics of Gd(III) spin labels for the study of protein conformations. in *Methods in Enzymology, chapter 8* 235–290 (2021).
4. Clayton, J. A. *et al.* Quantitative analysis of zero-field splitting parameter distributions in Gd(III) complexes. *PCCP Phys. Chem. Chem. Phys.* **20**, 10470–10492 (2018).
5. Shah, A. *et al.* A Gadolinium Spin Label with Both a Narrow Central Transition and Short Tether for Use in Double Electron Electron Resonance Distance Measurements. *Inorg. Chem.* **58**, 3015–3025 (2019).
6. Edwards, D. T. *et al.* Extending the distance range accessed with continuous wave EPR with Gd3+spin probes at high magnetic fields. *PCCP Phys. Chem. Chem. Phys.* **15**, 11313–11326 (2013).
7. Clayton, J. A. *et al.* Gd3+–Gd3+ distances exceeding 3 nm determined by very high frequency continuous wave electron paramagnetic resonance. *PCCP Phys. Chem. Chem. Phys.* **19**, 5127–5136 (2017).
8. Maity, S. *et al.* Triggered Functional Dynamics of AsLOV2 by Time-Resolved Electron Paramagnetic Resonance at High Magnetic Fields. *Angew. Chem. Int. Ed.* **1**, 1–1 (2023).
9. Gan, Z. *et al.* NMR spectroscopy up to 35.2 T using a series-connected hybrid magnet. *J. Magn. Reson.* **284**, 125–136 (2017).
10. Benmelouka, M. *et al.* A High-Frequency EPR Study of Frozen Solutions of GdIII Complexes: Straightforward Determination of the Zero-Field Splitting Parameters and Simulation of the NMRD Profiles. *JACS* **128**, 7807–7816 (2006).
11. Krzystek, J., Sienkiewicz, A., Pardi, L. & Brunel, L. C. DPPH as a Standard for High-Field EPR. *J. Magn. Reson.* **125**, 207–211 (1997).
12. Wind, R. A., Duijvestijn, M. J., van der Lugt, C., Manenschijn, A. & Vriend, J. Applications of dynamic nuclear polarization in 13C NMR in solids. *Prog. Nucl. Magn. Reson. Spectrosc.* **17**, 33–67 (1985).
13. McKenna, A. M. *et al.* Expanding the Analytical Window for Biochar Speciation: Molecular Comparison of Solvent Extraction and Water-Soluble Fractions of Biochar by FT-ICR Mass Spectrometry. *Anal. Chem.* **93**, 15365–15372 (2021).
14. Bonanomi, G. *et al.* Biochar chemistry defined by 13C-CPMAS NMR explains opposite effects on soilborne microbes and crop plants. *Appl. Soil Ecol.* **124**, 351–361 (2018).
15. Gourier, D. *et al.* Extreme deuterium enrichment of organic radicals in the Orgueil meteorite: Revisiting the interstellar interpretation? *Geochim. Cosmochim. Acta* **72**, 1914–1923 (2008).
16. Chow, W. Y. *et al.* Pigmentation Chemistry and Radical-Based Collagen Degradation in Alkaptonuria and Osteoarthritic Cartilage. *Angew. Chemie - Int. Ed.* **59**, 11937–11942 (2020).
17. Becerra, L. R., Gerfen, G. J., Temkin, R. J., Singel, D. J. & Griffin, R. G. Dynamic nuclear polarization with a cyclotron resonance maser at 5 T. *Phys. Rev. Lett.* **71**, 3561–3564 (1993).
18. Hu, K.-N., Yu, H., Swager, T. M. & Griffin, R. G. Dynamic Nuclear Polarization with Biradicals. *J. Am. Chem. Soc.* **126**, 10844–10845 (2004).

19. Dane, E. L., Maly, T., Debelouchina, G. T., Griffin, R. G. & Swager, T. M. Synthesis of a BDPA-TEMPO biradical. *Org. Lett.* **11**, 1871–1874 (2009).
20. Mathies, G. *et al.* Efficient Dynamic Nuclear Polarization at 800 MHz/527 GHz with Trityl-Nitroxide Biradicals. *Angew. Chemie* **127**, 11936–11940 (2015).
21. Harrabi, R. *et al.* Highly Efficient Polarizing Agents for MAS-DNP of Proton-Dense Molecular Solids. *Angew. Chemie Int. Ed.* **61**, e2021141-1—e2021141-9 (2022).
22. Kubicki, D. J. *et al.* Rational design of dinitroxide biradicals for efficient cross-effect dynamic nuclear polarization. *Chem. Sci.* **7**, 550–558 (2016).
23. Wisser, D. *et al.* BDPA-Nitroxide Biradicals Tailored for Efficient Dynamic Nuclear Polarization Enhanced Solid-State NMR at Magnetic Fields up to 21.1 T. *J. Am. Chem. Soc.* **140**, 13340–13349 (2018).
24. Perras, F. A. *et al.* Methyl-Driven Overhauser Dynamic Nuclear Polarization. *J. Phys. Chem. Lett.* **13**, 4000–4006 (2022).
25. Delage-Laurin, L. *et al.* Overhauser Dynamic Nuclear Polarization with Selectively Deuterated BDPA Radicals. *J. Am. Chem. Soc.* **143**, 20281–20290 (2021).
26. Stoll, S. & Schweiger, A. EasySpin, a comprehensive software package for spectral simulation and analysis in EPR. *J. Magn. Reson.* **178**, 42–55 (2006).
27. Bennati, M. *et al.* Pulsed electron-nuclear double resonance (ENDOR) at 140 GHz. *J. Magn. Reson.* **138**, 232–243 (1999).
28. Neese, F. The ORCA program system. *Wiley Interdiscip. Rev. Comput. Mol. Sci.* **2**, 73–78 (2012).
29. Grimme, S., Brandenburg, J. G., Bannwarth, C. & Hansen, A. Consistent structures and interactions by density functional theory with small atomic orbital basis sets. *J. Chem. Phys.* **143**, 054107-1—054107-19 (2015).
30. Adamo, C. & Barone, V. Toward reliable density functional methods without adjustable parameters: The PBE0 model. *J. Chem. Phys.* **110**, 6158–6170 (1999).
31. Weigend, F. & Ahlrichs, R. Balanced basis sets of split valence, triple zeta valence and quadruple zeta valence quality for H to Rn: Design and assessment of accuracy. *Phys. Chem. Chem. Phys.* **7**, 3297–3305 (2005).
32. Mitchell, D. G. *et al.* Electron Spin Relaxation and Heterogeneity of the 1:1 r,γ-Bisdiphenylene-β-phenylallyl (BDPA)/Benzene Complex. *J. Phys. Chem. B* **115**, 7986–7990 (2011).
33. Raitsimring, A. M., Astashkin, A. V., Poluektov, O. G. & Caravan, P. High-field pulsed EPR and ENDOR of Gd3+ complexes in glassy solutions. *Appl. Magn. Reson.* **28**, 282–295 (2005).

Durham University
Durham Research Online

Citation on deposit: Dubroca, T., Wang, X., Mentink-Vigier, F., Trociewitz, B., Starck, M., Parker, D., …Krzystek, J. (2023). Terahertz EPR spectroscopy using a 36-tesla high-homogeneity series-connected hybrid magnet. Journal of Magnetic Resonance, 353, Article 107480. https://doi.org/10.1016/j.jmr.2023.107480

For final citation and metadata, visit Durham Research Online URL:
https://durham-repository.worktribe.com/output/2047571

Copyright statement: © 2023. This manuscript version is made available under the CC-BY-NC-ND 4.0 license https://creativecommons.org/licenses/by-nc-nd/4.0/